Eur Biophys J (2012) 41:723–732
DOI 10.1007/s00249-012-0848-y

ORIGINAL PAPER

EBSA
Biophysics in Europe

The role of carboxymethyl substituents in the interaction of tetracationic porphyrins with DNA

Oxana A. Kovaleva · Vladimir B. Tsvetkov · Anna K. Shchyolkina · Olga F. Borisova · Valentina A. Ol'shevskaya · Anton V. Makarenkov · Alexander S. Semeikin · Alexander A. Shtil · Dmitry N. Kaluzhny

Received: 23 May 2012 / Revised: 10 July 2012 / Accepted: 1 August 2012 / Published online: 19 August 2012
© European Biophysical Societies' Association 2012

Abstract Cationic porphyrin-based compounds capable of interacting with DNA are currently under extensive investigation as prospective anticancer and anti-infective drugs. One of the approaches to enhancing the DNA-binding affinity of these ligands is chemical modification of functional groups of the porphyrin macrocycle. We analyzed the interaction with DNA of novel derivatives containing carboxymethyl and ethoxycarbonylmethyl substituents at quaternary nitrogen atoms of pyridinium groups at the periphery of the porphyrin macrocycle. The parameters of binding of 5,10,15,20-tetrakis(*N*-carboxymethyl-4-pyridinium) porphyrin (P1) and 5,10,15,20-tetrakis(*N*-ethoxycarbonylmethyl-4-pyridinium)porphyrin (P2) to double-stranded DNA sequences of different nucleotide content were determined using optical spectroscopy. The association constant of P1 interaction with calf thymus DNA ($K = 3.4 \times 10^6$ M^{-1}) was greater than that of P2 ($K = 2.8 \times 10^5$ M^{-1}). Preferential binding of P1 to GC- rather than AT-rich oligonucleotides was detected. In contrast, P2 showed no preference for particular nucleotide content. Modes of binding of P1 and P2 to GC and AT duplexes were verified using the induced circular dichroism spectra. Molecular modeling confirmed an intercalative mode of interaction of P1 and P2 with CpG islands. The carboxyl groups of the peripheral substituent in P1 determine the specific interactions with GC-rich DNA regions, whereas ethoxycarbonylmethyl substituents disfavor binding to DNA. This study contributes to the understanding of the impact of peripheral substituents on the DNA-binding affinity of cationic porphyrins, which is important for the design of DNA-targeting drugs.

Keywords DNA · Porphyrins · Affinity · Absorption · Fluorescence · Molecular docking

O. A. Kovaleva · A. K. Shchyolkina · O. F. Borisova · D. N. Kaluzhny (✉)
Engelhardt Institute of Molecular Biology, Russian Academy of Sciences, Moscow 119991, Russia
e-mail: uzhny@mail.ru

O. A. Kovaleva
Moscow Institute of Physics and Technology, State University, Dolgoprudny 141700, Russia

V. B. Tsvetkov
Orekhovich Institute of Biomedical Chemistry, Russian Academy of Medical Sciences, Moscow 119121, Russia

V. B. Tsvetkov
Topchiev Institute of Petrochemical Synthesis, Russian Academy of Sciences, Moscow 119991, Russia

V. A. Ol'shevskaya · A. V. Makarenkov
Nesmeyanov Institute of Organoelement Compounds, Russian Academy of Sciences, Moscow 119991, Russia

A. S. Semeikin
Ivanovo State University of Chemistry and Technology, Ivanovo 153000, Russia

A. A. Shtil
Blokhin Cancer Center, Russian Academy of Medical Sciences, Moscow 115478, Russia

Introduction

Porphyrins and their derivatives are widely used in photodynamic therapy of tumors (Luo et al. 1996; Shieh et al. 2010; Tada-Oikawa et al. 2009) and beyond, also exerting antibacterial and antiviral effects (Ding et al. 1992; Steenkeste et al. 2010). Due to their unique photochemical properties, individual porphyrin-based compounds can be used as artificial endonucleases (Haeubl et al. 2009).

Cationic porphyrins are one of the well-studied classes of DNA ligands (Sari et al. 1990; Chirvony et al. 1997; Ford and Neidle 1995; Pasternack 2003; Tjahjono et al. 2001). These compounds are able to form various complexes with DNA. Peripheral substituents as well as metal ions in the porphyrin macrocycle significantly influence the mode of binding, that is, intercalation or binding to the DNA minor groove. Tetrakis-(*N*-methyl-4-pyridinium)porphyrin (TMPyP4), the cationic pyridinium derivative of porphyrin with methyl substituents at the positively charged nitrogen atom of the pyridinium ring, shows high affinity to double-helical DNA. Importantly, the primary DNA structure plays the decisive role in determining the mode of binding: TMPyP4 intercalates between GC base pairs and also interacts with AT base pairs in the DNA minor groove (Hui et al. 1990; Ford and Neidle 1995; Kim et al. 2004). Furthermore, a positive charge at the periphery of the porphyrin macrocycle plays a key role in porphyrin–DNA interactions. For example, tetracationic *para*-substituted pyridinium derivatives exhibit the highest affinity to DNA compared with *meta*- and *ortho*-substituted methyl pyridinium porphyrins (Sari et al. 1990; Dutikova et al. 2010). The presence of a central metal ion in the macrocycle greatly affects the type of binding and the affinity to DNA (Tjahjono et al. 2001).

In search of optimized porphyrin-based DNA ligands, new derivatives with various moieties at the periphery of the cationic porphyrin have been synthesized (Frau et al. 1997; Biron and Voyer 2005; Garcia et al. 2009; Mezo et al. 2011; Berezin et al. 2007). Introduction of carboxymethyl and ethoxycarbonylmethyl substituents resulted in increased water solubility due to the relatively large volume of the substituents and the decreased energy of the crystalline state of these compounds (Berezin et al. 2007). However, thermodynamic parameters of binding of these ligands to DNA remained unknown. In the present study we examined the effect of carboxymethyl and ethoxycarbonylmethyl substituents at the periphery of tetracationic pyridinium porphyrin (Fig. 1) on their affinity to DNA of different nucleotide content. We also elucidated the role of the carboxyl groups in these substituents in drug–DNA interaction and analyzed the types of the complexes formed by the new compounds and DNA.

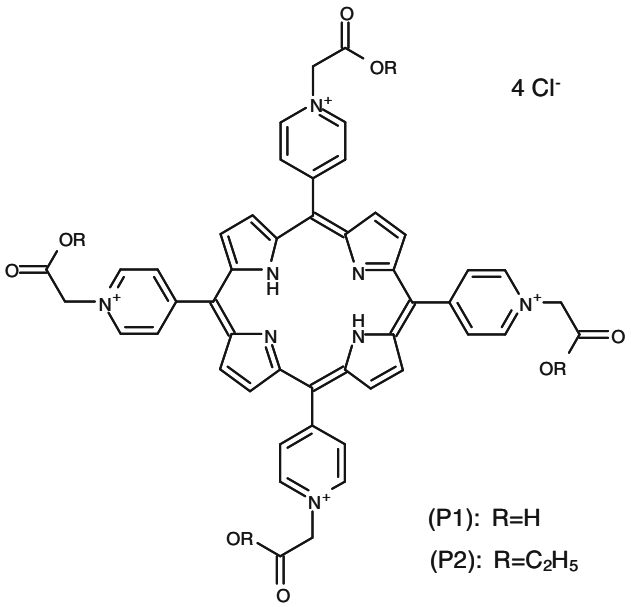

Fig. 1 Derivatives of 5,10,15,20-tetrakis(4-*N*-pyridinium)porphyrin with peripheral carboxymethyl and ethoxycarbonylmethyl substituents

Materials and methods

Reagents

5,10,15,20-Tetrakis(*N*-carboxymethyl-4-pyridinium)porphyrin tetrachloride (P1) and 5,10,15,20-tetrakis(*N*-ethoxycarbonylmethyl-4-pyridinium)porphyrin tetrachloride (P2) (Fig. 1) were synthesized in Ivanovo State University of Chemistry and Technology (Berezin et al. 2007) by alkylation of *meso*-5,10,15,20-tetrapyridylporphyrin with chloroacetic acid (P1) or ethyl chloroacetate (P2) in refluxing dimethylformamide.

Calf thymus DNA (ctDNA) was purchased from Sigma-Aldrich, USA. Oligonucleotides $d(AT)_{20}$ and $d(GC)_{20}$ were synthesized and high-performance liquid chromatography (HPLC)-purified by Lytech, Moscow. Concentrations of the oligonucleotides in aqueous solutions were determined based on ultraviolet (UV) absorbance at 260 nm, 90 °C. The following molar extinction coefficients were used: $\varepsilon[d(AT)_{20}] = 10{,}250\ M(N)^{-1}\ cm^{-1}$ and $\varepsilon[d(GC)_{20}] = 8{,}000\ M(N)^{-1}\ cm^{-1}$. The concentration of ctDNA (moles of nucleotides, N) was determined in sodium phosphate buffered solution at 20 °C using the molar extinction coefficient $\varepsilon[ctDNA] = 6{,}600\ M(N)^{-1}\ cm^{-1}$. Stock solutions of P1 and P2 (100 μM each) were prepared by dissolving the dry compounds in water. Oligonucleotides $d(AT)_{20}$ and $d(GC)_{20}$ were heated to 90 °C and then slowly cooled down to room temperature to form double-stranded DNAs (AT and GC duplexes, respectively). The porphyrin–DNA complexes were formed at 20 °C in solutions containing 1 μM of P1 or P2, 20 μM (N) of ctDNA or oligonucleotides, 100 mM NaCl, and 10 mM sodium phosphate, pH 7.8.

Instruments

The absorption spectra of the porphyrin–DNA complexes were recorded in the 350–500 nm wavelength region using a Jasco V-550 spectrophotometer. Fluorescence emission

spectra were registered with a Cary Eclipse spectrofluorimeter (Varian) over the wavelength region of 600–800 nm. The excitation wavelength was $\lambda = 435$ nm. Fluorescence decay curves were obtained using EasyLife V^{TM} (OBB) upon excitation with a pulsed light-emitting diode (LED) with peak emission at 435 nm. A filter transmitting at wavelengths above 590 nm was used. Fluorescence lifetimes (τ) were calculated with FelixGX software using mono- or biexponential decay laws. The results of three measurements of lifetime were averaged. Circular dichroism (CD) spectra in the 220–480 nm region were recorded using a Jasco-715 spectropolarimeter.

Quantum yield of fluorescence

The relative quantum yield of fluorescence was calculated using absorption and fluorescence emission spectra. Areas under the curves of fluorescence spectra were normalized to units of absorbed photons (Borisova et al. 1991; Magde et al. 2002). The absolute quantum yield was estimated relative to a solution of carboxyfluorescein (Magde et al. 2002) (see "Results and discussion").

Adsorption isotherms

The adsorption isotherms of P1 and P2 were generated from ligand absorption at $\lambda = 422$ nm upon titration with DNA of various nucleotide content. The following concentrations were used: P1 (1 μM) was titrated with ctDNA [2–100 μM (N)] or the GC duplex [0.8–50 μM (N)]; P1 (14 μM) was titrated with the AT duplex [10–400 μM (N)]; P2 (1 μM) was titrated with ctDNA [2.4–110 μM (N)] and with the GC duplex (0.8–8.1 μM); P2 [16 μM (N)]—with the AT duplex [10–400 μM (N)]. Changes in concentrations due to dilution were taken into account. The concentration of the bound ligand at $\lambda = 422$ nm was calculated by the equation

$$C_b = \frac{\varepsilon - \varepsilon_f}{\varepsilon_b - \varepsilon_f} \times C_0, \quad (1)$$

where C_0 is the concentration of a ligand in the sample, and ε, ε_f and ε_b are the molar extinctions of the ligand in the sample, free ligand, and bound ligand, respectively. The association constant K was determined by approximation of experimental isotherms constructed in Scatchard coordinates with the equation describing the model of independent binding of the extended ligand to a linear lattice (McGhee and von Hippel 1974):

$$\frac{r}{C_f} = K(1 - n \cdot r)\left(\frac{1 - n \cdot r}{1 - (n-1) \cdot r}\right)^{(n-1)}, \quad (2)$$

where K is the association constant, r is the average number of bound ligand molecules per one base pair $r = C_b/C_{DNA}$, and n is the number of base pairs bound to one molecule of the ligand (exclusion length).

Molecular modeling of porphyrin–DNA complex

The atomic position coordinates of the DNA duplex were taken from nuclear magnetic resonance (NMR) data of the intercalative complex with ellipticine (PDB ID: 1Z3F). Partial atomic charges on DNA atoms were determined by the Gasteiger–Hückel method (Gasteiger and Marsili 1978) using SYBYL 8 (SYBYL 8.0, Tripos International, 1699 South Hanley Rd., St. Louis, Missouri, 63144, USA) molecular graphics software package. Unfavorable van der Waals interactions in the duplex structure were removed by short minimizations using SYBYL 8.0 and the Powell (1977) method with the following parameters: TRIPOS force field, nonbond distance cutoff of 8 Å, the distance-dependent dielectric function, simplex initial optimization, convergence threshold of 0.05 kcal/mol Å, and cutoff for iterations of 500 cycles. The distance constraints were applied to the H-bond donor and acceptor atoms to preserve the H-bond network in the minimization procedures. Partial atomic charges on ligand atoms were calculated by the PM3 (Stewart 2007) quantum-mechanical semi-empirical method by the application of the MOPAC 7.0 package included in Vega ZZ (Pedretti et al. 2004).

To define the most probable binding site for the ligand in the duplex, the procedure of flexible ligand docking to the full surface of a rigid duplex was performed using AUTODOCK 4.2 (Morris et al. 2009). Preparation of the target and ligands for docking was performed using the program AutoDockTools (ADT version 1.5.4), in which the partial atomic charges on the ligand's and target's atoms were preserved. The grid maps of docking studies were computed using AutoGrid4. The grid center was placed at the target center, and 90 × 90 × 90 points with grid spacing of 0.375 were calculated. The genetic algorithm local search (GA-LS) method was applied to find the most probable binding site. The following parameters for GA-LS were used: number of GA runs 10, maximal number of energy evaluations 250,000, maximal number of generations 27,000, and mutation and crossover rates of 0.02 and 0.8, respectively. Pseudo-Solis & Wets parameters were used for local search; the number of iterations was set to 300. The starting position and conformation of ligands were random. The step of rotation of torsion angle was equal to 50°. After docking, all generated structures were clustered up with root mean square (RMS) tolerance of 2 Å from the lowest-energy structure. The DNA–ligand complex was visualized using Chimera v1.5.3 (Pettersen et al. 2004).

Results and discussion

Interaction of P1 and P2 with DNA detected by UV absorption spectroscopy

Formation of complexes of P1 and P2 with ctDNA, GC and AT duplexes was detected by changes in the absorption spectra of porphyrins in the Soret band, $380 < \lambda < 480$ nm. P1 and P2 demonstrated similar optical properties under our experimental conditions. The absorption spectra of free P1 and P2 molecules (Fig. 2, open circles) showed a maximum at $\lambda = 422$ nm with molar extinction coefficient $\varepsilon = (2.2 \pm 0.1) \times 10^5$ M^{-1} cm^{-1}. Binding of P1 and P2 to DNAs caused a long-wavelength (bathochromic) shift in the absorption spectra, while the intensities of the absorption bands decreased (a hypochromic effect) (Fig. 2). The observed spectral changes are characteristic of porphyrin–DNA interactions (Hui et al. 1990; Ford and Neidle 1995; Kim et al. 2004; Sari et al. 1990).

Interaction of P1 and P2 with ctDNA (Fig. 2a, d) caused a bathochromic shift (11 and 7 nm, respectively). The hypochromic effect upon binding to ctDNA was similar for both compounds. Typically, the extinction values of cationic porphyrins at their absorption maximum are reduced by a factor of 1.7 upon binding to ctDNA. A certain imprecision of the isosbestic point at $\lambda \approx 436$ nm (Fig. 2a) suggests the presence of a minor, spectrally different form(s) along with the main form of P1 bound to ctDNA. This may be due to the interaction of P1 with ctDNA regions of different nucleotide content.

To obtain spectral characteristics of complexes formed by P1 and P2 with AT- and GC-rich DNA, we used AT and GC duplexes. A considerable bathochromic shift ($\sim$22 nm) in the absorption spectra occurred upon P1 and P2 complexation with the GC duplex (Fig. 2b, e). Figure 2 shows a twofold decrease of extinction at the absorption maximum upon P1 binding to this duplex.

Formation of P1 and P2 complexes with the AT duplex (Fig. 2c, f) was accompanied by an 8 nm bathochromic shift. This effect was similar for both compounds; for P2 there was also a slight hypochromic effect. Of note, spectral changes upon interaction of P1 or P2 with GC and AT duplexes were characterized by isosbestic points at 438 and 427 nm, respectively, suggesting a single particular type of complexes formed by P1 and P2 with AT or GC duplexes.

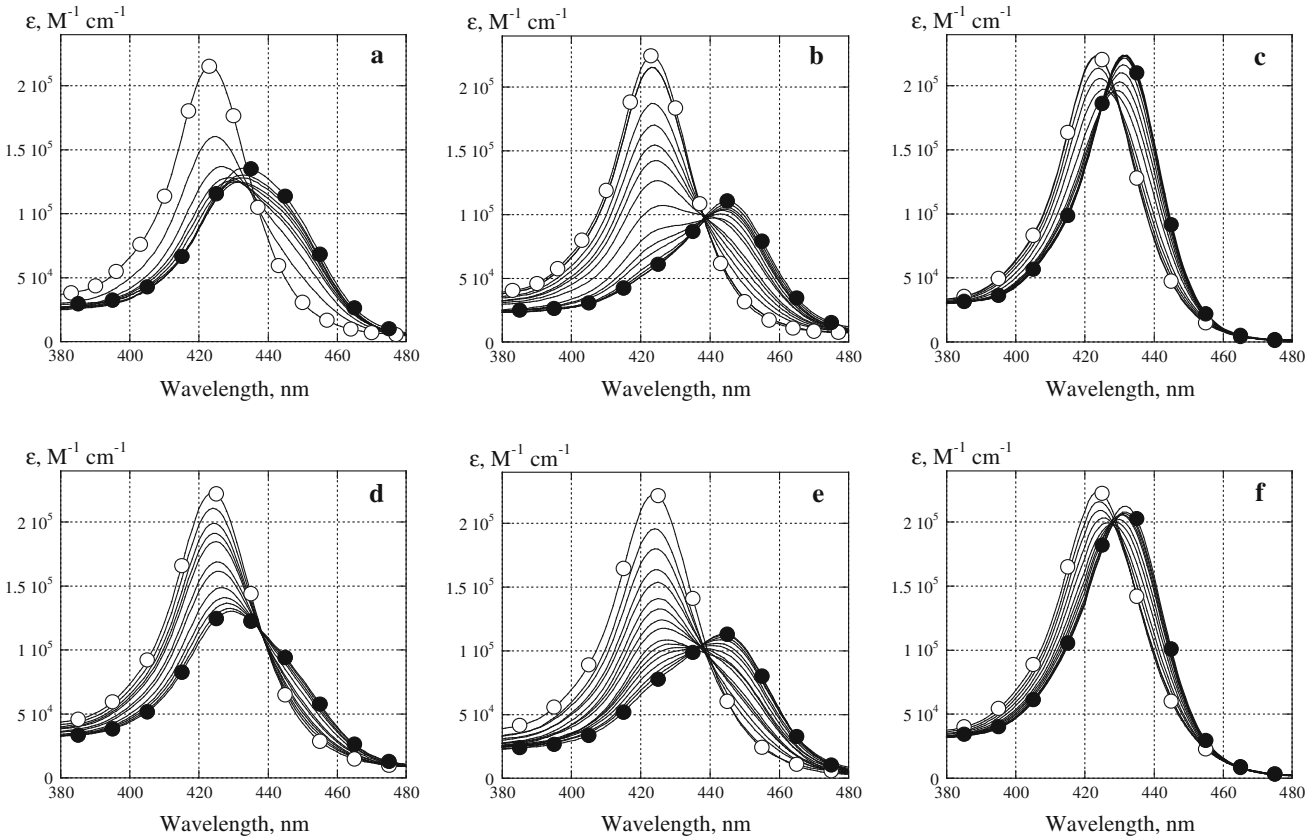

Fig. 2 Changes in absorption spectra (Soret band) of P1 and P2 upon addition of DNA. Titration of P1 with: **a** ctDNA, **b** GC duplex, **c** AT duplex. Titration of P2 with: **d** ctDNA, **e** GC duplex, **f** AT duplex. *Open circles* spectra of free compounds, *filled circles* spectra of DNA–ligand complexes

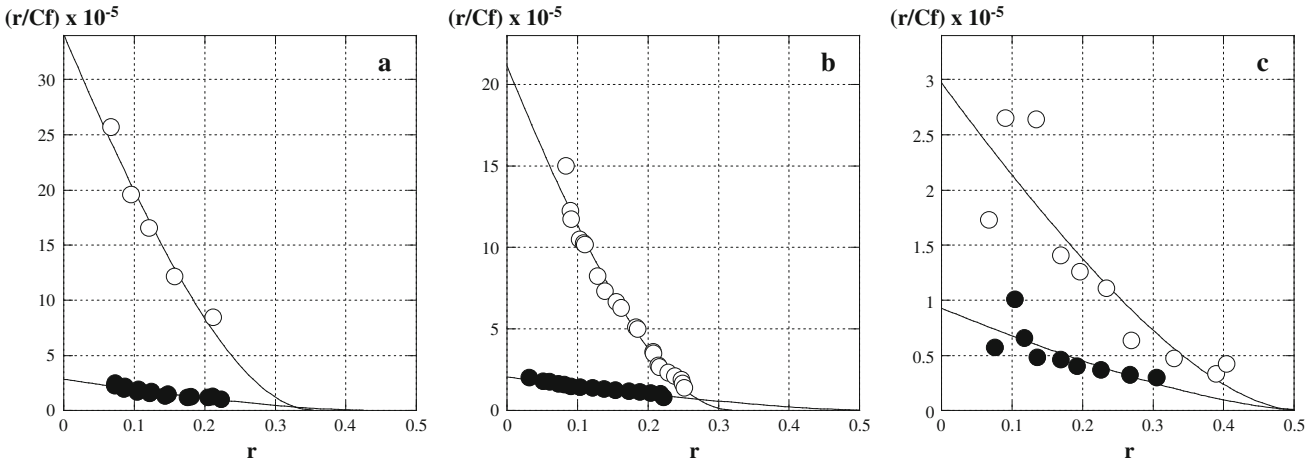

Fig. 3 Isotherms of P1 (*open circles*) and P2 (*filled circles*) binding with DNA of different base content. **a** ctDNA, **b** GC duplex, **c** AT duplex

Table 1 Parameters of binding of P1 and P2 to DNA of various base content

Cmpd	ctDNA		GC duplex		AT duplex	
	K, 10^5 M^{-1}	n, bp	K, 10^5 M^{-1}	n, bp	K, 10^5 M^{-1}	n, bp
P1	34.1 ± 2.0	2.7 ± 0.2	21.1 ± 0.6	3.0 ± 0.1	3.0 ± 0.4	2.0 ± 0.2
P2	2.8 ± 0.2	2.2 ± 0.1	2.1 ± 0.1	1.9 ± 0.1	1.0 ± 0.2	1.9 ± 0.3

Parameters of P1 and P2 binding to DNA

The adsorption isotherms in Scatchard coordinates are given in Fig. 3a–c. The shapes of the binding curves (Fig. 3) indicate an anticooperative mode of ligand binding to DNA. Approximation of the experimental points with Eq. (2) (see "Materials and methods") provided the association constant values (K) and exclusion lengths (n) (Table 1).

The P1 and P2 molecules bound to ctDNA occupied approximately 3 and 2 bp, respectively (Table 1). It is noteworthy that P2 carries bulkier substituents in its side-groups but occupies fewer base pairs on ctDNA than P1, perhaps because the substituents in the side-groups of P2 do not interact with DNA.

Most importantly, P1 showed the greatest affinity to ctDNA and the GC duplex. The association constants of P1 are much larger than those of P2 for the complexes with the respective DNAs. One may hypothesize that the formation of additional bonds between the side-substituents of P1 and DNA can increase the affinity of P1 to ctDNA and the GC duplex. Furthermore, P1 demonstrated stronger preference for binding to GC pairs than to AT pairs (Table 1). The association constant of the P1 complex with the GC duplex is seven times greater than that of the complex P1:AT duplex. In contrast, P2 demonstrated lower preference for the GC duplex: the K value for the GC duplex was only twofold greater than for the AT duplex. Preference for GC base pairs is typical for intercalative ligands (Borissova et al. 1972). Interestingly, the affinity of P1 and P2 to ctDNA was somewhat greater than to the GC duplex (Table 1), probably due to preferential intercalation of the ligands into an alternative favorable site, namely, a 5′-TpG stacking contact (Jain and Rajeswari 2002). Thus, we showed that the carboxyl groups of P1 confer increased affinity for GC-rich DNA regions. The carboxyl group may be a hydrogen bond donor, thereby contributing to the increased P1 binding to DNA.

The K value of P1 is compatible with the association constant of the porphyrin derivative TMPyP4 with ctDNA (4–6 × 10^6 M^{-1}, a value approximated for corresponding ionic conditions) (Sari et al. 1990; Strickland et al. 1988). At the same time, TMPyP4 did not demonstrate any preference for GC pairs. We conclude that the carboxymethyl group determines the specificity of the interaction between porphyrins and GC-rich DNA regions.

Modes of P1 and P2 binding to DNA duplexes

The modes of binding of P1 and P2 to GC and AT duplexes and ctDNA were determined by the induced CD bands in the Soret region (Fig. 4). The sign of the induced CD signal in the Soret region, a marker of a porphyrin binding mode for synthetic polynucleotides, can be extended to natural DNAs at low drug occupancies (Pasternack 2003). The critical angle for the CD signal change in the Soret region lies between porphyrin orientation perpendicular to the helix axis (as for an intercalative complex) and a porphyrin

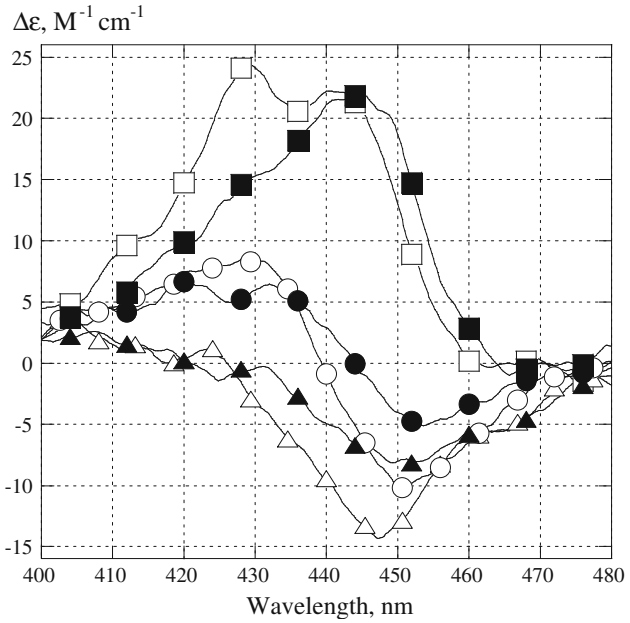

Fig. 4 CD spectra in the Soret region of P1 (*open markers*) and P2 (*filled markers*) in complexes with ctDNA (*circles*), GC duplex (*triangles*), and AT duplex (*squares*). Concentrations: DNA duplexes 20 μM (N), porphyrins 3 μM

nestled in a minor groove of a double helix (Pasternack 2003). Figure 4 shows that the induced CD signals of P1 and P2 in the Soret region are close. Binding to the AT duplex results in a positive induced CD signal (Fig. 4, squares), while the binding to the GC duplex brings about a negative signal (Fig. 4, triangles). The shapes of induced CD spectra of P1 and P2 bound to ctDNA represent a mixture of positive and negative bands (Fig. 4, circles). These data indicate the intercalative mode of binding of P1 and P2 to the GC duplex and the groove binding of these porphyrins to the AT duplex. Binding to ctDNA includes both intercalative and groove-binding modes.

Fluorescence of complexes of P1 and P2 with DNA duplexes

The fluorescence emission spectra of free and bound P1 and P2 are shown in Fig. 5. The fluorescence intensities of free P1 and P2 were close to those of the ctDNA-bound compounds. However, the shapes of the spectra changed dramatically: the fluorescence intensity was redistributed between 655 and 715 nm bands. The more pronounced peaks in the fluorescence spectra indicate limited vibrational degrees of freedom of the fluorophore upon binding to DNA.

The fluorescence intensity of each compound reduced more than threefold upon binding to the GC duplex (Fig. 5, triangles). This effect is typical for many intercalative ligands whose fluorescence is quenched due to complex formation with charge transfer (Jain and Rajeswari 2002; Borissova et al. 1972; Jasuja et al. 1997). The fluorescence spectra of P1 and P2 bound to the GC duplex showed band shifts from 655 to 665 nm and from 715 to 730 nm, respectively (Fig. 5, filled circles and triangles). Thus, P1 and P2 binding to the GC duplex forms weakly fluorescent complexes quenched by GC base pairs. The fluorescence intensity of P1 and P2 increased five- to sixfold due to interaction with the AT duplex. The intensities of the fluorescence bands at 655 and 715 nm increased (Fig. 5, squares). As for the porphyrin–GC binding, the distinct maxima in the fluorescence spectra of AT-bound ligands argue for the restricted vibrational degrees of freedom of the fluorophores (Chirvony et al. 1997).

Fluorescence lifetimes and quantum yields of P1 and P2 complexes with DNA duplexes

Absolute fluorescence quantum yields (q_0) of P1 and P2 in buffer solution were calculated relative to the known fluorescence quantum yield of carboxyfluorescein (Magde et al. 2002) ($q_{fl} = 0.93$): $q_0 = 0.0093$ for P1 and $q_0 = 0.0086$ for P2. Fluorescence quantum yields (q) of P1 and P2 complexes with DNA were calculated and are presented as q/q_0 in Table 2. The q/q_0 values of P1 and P2 changed slightly upon binding to ctDNA, increased two-fold in complexes with the AT duplex, and decreased by factors of 3.5 and 2, respectively, in complexes with the GC duplex. These data indicate that the formation of the complexes with GC base pairs led to significant quenching of fluorescence of both P1 and P2. Similar results have been reported for TMPyP4 (Chirvony et al. 1997).

To clarify the mechanism of the fluorescence change upon P1 and P2 binding to DNA of different base content, we studied the fluorescence decay kinetics (Fig. 6). The experimental conditions provided mean occupancy $r \leq 0.1$; the unbound ligand concentration did not exceed 2 % for P1 or 10 % for P2. For detailed characterization of the fluorescence decay, deconvolution of the experimental curves and their approximation with one- or two-exponential decay equations were performed. Table 2 shows the calculated fluorescence decay times of the first and second components (τ_1 and τ_2) and their proportions (a_1 and a_2) that are dependent on the concentration of each component. The τ_i/τ_0 values calculated relatively to free ligand (τ_0) are given for comparison with the fluorescence quantum yield q/q_0 in Table 2.

The fluorescence decay curves of unbound P1 and P2 fitted well with a mono-exponential equation. This fitting corresponds to a single fluorescent form of P1 and P2 in aqueous solution. The fluorescence lifetimes of free P1 and P2 molecules were the same within experimental error: $\tau_0 = 4.8 \pm 0.1$ and $\tau_0 = 4.6 \pm 0.1$ ns, respectively.

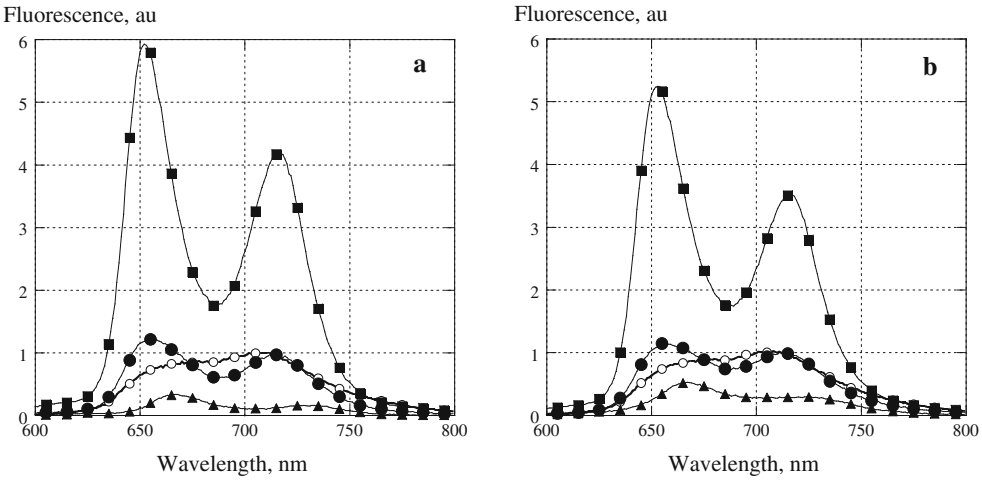

Fig. 5 Fluorescence emission spectra of free and DNA-bound P1 (**a**) and P2 (**b**). Fluorescence emission of free compounds (*open circles*), complexes with ctDNA (*filled circles*), GC duplex (*filled triangles*), and AT duplex (*filled squares*). Excitation wavelength $\lambda_{ex} = 435$ nm. The fluorescence intensity of the free compound at 715 nm was taken as a unit. The concentrations of P1 and P2 were 1 μM, DNAs: 20 μM (N)

Table 2 Lifetimes and fluorescence quantum yields of P1 and P2 complexed with DNA

	τ_1, ns	a_1	τ_1/τ_o	τ_2, ns	a_2	τ_2/τ_o	q/q_o
P1							
Free	4.8 ± 0.1	1	1.00				1
dsAT	10 ± 0.2	1	2.08				2.2
dsGC	0.7 ± 0.1	0.65	0.15	5.3 ± 0.2	0.35	1.10	0.28
ctDNA	0.7 ± 0.1	0.47	0.15	10 ± 0.3	0.53	2.08	0.85
P2							
Free	4.6 ± 0.1	1	1.00				1
dsAT	8.6 ± 0.1	1	1.87				2.0
dsGC	0.6 ± 0.1	0.61	0.13	4.2 ± 0.2	0.39	0.91	0.48
ctDNA	0.5 ± 0.1	0.52	0.11	8.1 ± 0.2	0.49	1.76	0.92

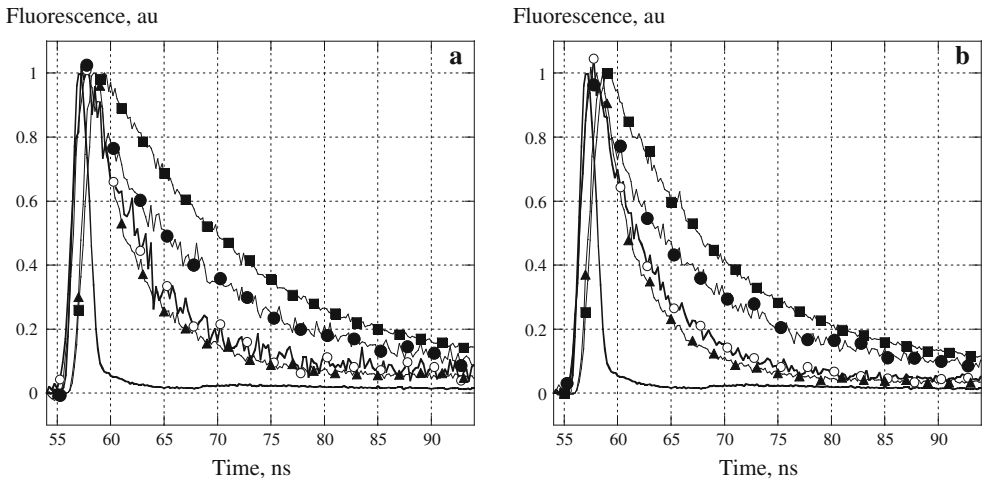

Fig. 6 Fluorescence decay curves of P1 (**a**) and P2 (**b**) for: free compounds (*open circles*), complexes with ctDNA (*filled circles*), complexes with GC duplex (*filled triangles*), and complexes with AT duplex (*filled squares*). *Solid curve* is an instrument response factor. Fluorescence intensity at the maximum of decay curves was taken as a unit

Slightly different lifetimes of P1 and P2 are consistent with absolute quantum yields of fluorescence (see above). The fluorescence decay curves of P1 and P2 bound to the AT duplex can be described by a mono-exponential equation. Fluorescence lifetimes (τ) increased approximately twofold compared with τ_0 of free molecules: $\tau = 10 \pm 0.2$ ns for P1:AT duplex and $\tau = 8.6 \pm 0.1$ ns for P2:AT duplex (Table 2). A twofold increase in the fluorescence lifetime corresponds to the same increase in the quantum yield of fluorescence of P1 and P2 bound to the AT duplex (Table 2). Such an increase in q and τ may be due to restriction of vibrational degrees of freedom of bound fluorophores and their shielding from water molecules.

The fluorescence decay curves of P1 and P2 bound to the GC duplex were fitted with a two-exponential equation. The fluorescence decay times (τ_1) of the short-lived component of P1 and P2 complexes with the GC duplex were 0.7 ± 0.1 and 0.6 ± 0.1 ns, respectively, with a large proportion of the short-lived component (60–65 %). Lifetimes of the long-lived component (τ_2) of P1 and P2 bound to the GC duplex (5.3 and 4.2 ns, respectively) were close to τ_0 of free ligands in solution. The presence of the short-lived component is consistent with a charge-transfer complex between GC pairs and the intercalated porphyrin (Chirvony et al. 1997; Borissova et al. 1972).

The presence of two types of complexes is evident from the fluorescence decay curves. The lifetimes of the short-lived components, 0.7 ± 0.1 and 0.6 ± 0.1 ns, for P1 and P2, respectively, were consistent with the interaction of the ligands with GC pairs and the formation of the charge-transfer complexes. The lifetimes of the long-lived components, 10.0 ± 0.3 and 8.1 ± 0.2 ns, for P1 and P2, respectively, coincided with the lifetimes of the complexes with the AT duplex (Table 2).

Thus, the fluorescence characteristics of P1 and P2 complexes with DNAs differed depending on the nucleotide content. Our data provide evidence for intercalative complexation with the GC duplex and for groove binding with the AT duplex. Heterogeneity of P1 and P2 complexes with a mixed DNA sequence arises from different modes of binding to GC contacts and to AT-rich regions.

Molecular modeling of interaction of P1 and P2 with dsDNA

To illustrate the intercalative type of complexes of P1 and P2 with $d(GC)_{20}$, we performed molecular modeling of these interactions (Fig. 7). The coordinates of a DNA complex with ellipticine were chosen for docking (PDB ID: 1Z3F). In that complex, the ellipticine molecule intercalates into a CpG stacking contact. The ellipticine molecules were removed from the DNA structure, and the DNA coordinates were used as a rigid target for docking. The scoring function values for the energy of DNA–ligand interaction were calculated for different ligand conformers formed during the docking procedure and located in various positions on the DNA surface. The solvent effect was taken into account. The value of the estimated energy for the intercalative complex appeared to be more advantageous than those for any other positioning of the ligand, and the conformers of nonintercalative binding were excluded from further consideration. Figure 7 presents the best pose of P1 (left) and P2 (right) docked into a CGA:TCG DNA region. The model shows the best complex with porphyrins intercalated into the space previously occupied by ellipticine. The resulting complex is stabilized by π-electron interactions between the porphyrin macrocycle and GC pairs, as well as by electrostatic interactions between positively charged nitrogen atoms of the porphyrin's pyridinium ring and DNA phosphates. Furthermore, the formation of three hydrogen bonds by carboxyl groups of P1 is suggested in the model. Two hydrogen bonds between P1 carboxyl groups and the phosphate oxygen of cytosines (in different strands) were observed. We also suggest the formation of an additional H-bond due to the proximity of the P1 carboxyl group to O5 of the adenine sugar. Thus, three carboxyl groups of P1 are able to interact with DNA, whereas the fourth carboxyl group is located at a considerable distance from DNA. On the other hand, no hydrogen bonds in the P2 intercalative complex were observed. The estimated interaction energy for the best porphyrin:DNA complex was -10.6 kcal/M ($K_i = 16$ nM) for P1 and -9.13 kcal/M ($K_i = 203$ nM) for P2. The calculated inhibition constants K_i are consistent with the experimental values derived from the spectroscopy data.

The model portrays the intercalation of P1 and P2 into a CpG island from the major groove (Fig. 7); one free carboxyl group of P1 projects into the major groove. Given that the carboxyl groups of P1 are located far from DNA bases, one can assume that the observed preference for GC-rich regions may be attributed to the cost-effective π-electron interactions of the porphyrin macrocycle with GC pairs. This assumption is in agreement with the data reported for other derivatives of cationic porphyrins (Hui et al. 1990).

Conclusions

The effects of carboxyl substituents on the interactions of cationic porphyrins with double-helical DNA of different nucleotide content were studied using absorption and fluorescence spectroscopy, and measurements of fluorescence quantum yield and lifetime. The association constant of P1 complexes with ctDNA (3.4×10^6 M^{-1}) was found to be considerably greater than that of P2:ctDNA

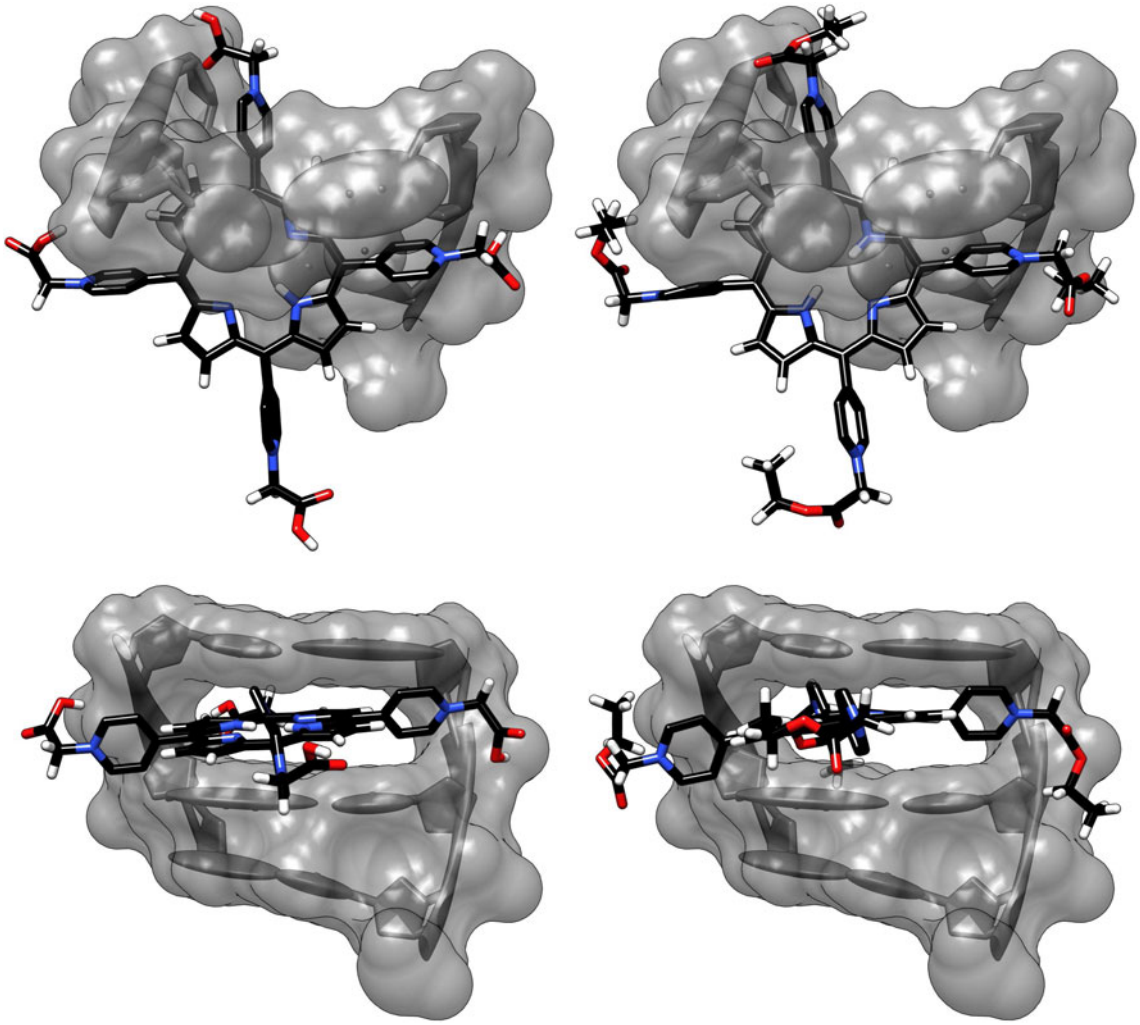

Fig. 7 Docking of P1 (*left*) and P2 (*right*) into a CGA:TCG DNA region. *Top* view parallel to the helical axis; *bottom* view from the major groove. DNA is presented schematically; the surface corresponding to van der Waals radii of DNA atoms is shown in *translucent gray*. The carbon atoms in porphyrins are depicted in *black*, the hydrogen atoms in *white*, nitrogen in *blue*, and oxygen in *red*

complexes (2.8×10^5 M^{-1}). Furthermore, preferential binding to guanine-rich DNA regions was demonstrated for P1, and the intercalative mode of P1 and P2 binding to GC stacking contacts was verified. Both compounds bound to the minor grooves of AT stretches. A possibility of complex formation with electron transfer was shown for P1 and P2 intercalation between GC base pairs.

Using the docking procedure, we built a model of interaction of P1 and P2 with the double helix CGA:TCG. The model supported the intercalative mode of binding. Apparently, the bulky substituents at the positively charged nitrogen atom in the pyridinium ring of the porphyrin may hinder groove binding of P1 and P2 to the CGA:TCG region. We identified chemical moieties at the periphery of the porphyrin macrocycle involved in interaction with DNA. Importantly, the carboxyl groups of the substituent in P1 determine a specific interaction with GC-rich regions of DNA. On the contrary, ethoxycarbonylmethyl substituents at the periphery of the tetracationic pyridinium porphyrin make binding to DNA less favorable.

A significant preference of P1 for GC-rich DNA regions and the formation of additional hydrogen bonds between carboxyl groups and DNA make possible a directional effect of the compound on different genome regions. It should be emphasized that one out of four carboxyl groups in P1 does not participate in interaction with DNA. This moiety can be used for chemical modifications to generate novel high-affinity DNA-targeting derivatives of porphyrins.

Acknowledgments The authors thank O. Mamaeva for assistance in CD measurements. This study was supported by the Russian Foundation for Basic Research (grant 12-04-00929-a).

References

Berezin M, Berezina N, Semeikin A, V'yugin A (2007) Thermochemistry of solution of some quaternized derivatives of tetra(4-pyridyl)porphine in water. Russ J Gen Chem 77(11):1955–1958. doi:10.1134/S1070363207110199

Biron E, Voyer N (2005) Synthesis of cationic porphyrin modified amino acids. Chem Commun (Camb) (37):4652–4654. doi:10.1039/b508380j

Borisova O, Golova Y, Gottikh B, Zibrov A, Il'icheva I, Lysov Y, Mamayeva O, Chernov B, Chernyi A, Shchyolkina A (1991) Parallel double stranded helices and the tertiary structure of nucleic acids. J Biomol Struct Dynam 8(6):1187–1210

Borissova OF, Potapov AP, Surovaya AN, Trubitsyn SN, Volkenstein MV (1972) The dependence of fluorescence quantum yield of the tRNA-acriflavine complexes on the conformational changes in tRNA. FEBS Lett 27(1):167–170

Chirvony VS, Galievsky VA, Kruk NN, Dzhagarov BM, Turpin P-Y (1997) Photophysics of cationic 5, 10, 15, 20-tetrakis-(4-N-methylpyridyl) porphyrin bound to DNA, [poly(dA-dT)]2 and [poly(dG-dC)]2: on a possible charge transfer process between guanine and porphyrin in its excited singlet state. J Photochem Photobiol B 40(2):154–162. doi:10.1016/s1011-1344(97)00043-2

Ding L, Balzarini J, Schols D, Meunier B, de Clercq E (1992) Anti-human immunodeficiency virus effects of cationic metalloporphyrin-ellipticine complexes. Biochem Pharmacol 44(8):1675–1679. doi: 10.1016/0006-2952(92)90486-3

Dutikova IuV, Borisova OF, Shchelkina AK, Lin J, Huang S, Shtil AA, Kaliuzhnyi DN (2010) 5, 10, 15, 20-Tetra-(N-methyl-3-pyridyl)porphyrin destabilizes the anti-parallel telomeric quadruplex d(TTAGGG)4. Mol Biol (Mosk) 44(5):929–937

Ford KG, Neidle S (1995) Perturbations in DNA structure upon interaction with porphyrins revealed by chemical probes, DNA footprinting and molecular modelling. Bioorg Med Chem 3(6):671–677. doi:10.1016/0968-0896(95)00052-i

Frau S, Bernadou J, Meunier B (1997) Nuclease activity and binding characteristics of a cationic "manganese porphyrin-bis(benzimidazole) dye (Hoechst 33258)" conjugate. Bioconjug Chem 8(2):222–231. doi:10.1021/bc970007e

Garcia G, Sarrazy V, Sol V, Le Morvan C, Granet R, Alves S, Krausz P (2009) DNA photocleavage by porphyrin-polyamine conjugates. Bioorg Med Chem 17(2):767–776. doi:10.1016/j.bmc.2008.11.047

Gasteiger J, Marsili M (1978) A new model for calculating atomic charges in molecules. Tetrahedron Lett 19(34):3181–3184. doi:10.1016/s0040-4039(01)94977-9

Haeubl M, Reith LM, Gruber B, Karner U, Muller N, Knor G, Schoefberger W (2009) DNA interactions and photocatalytic strand cleavage by artificial nucleases based on water-soluble gold(III) porphyrins. J Biol Inorg Chem 14(7):1037–1052. doi:10.1007/s00775-009-0547-z

Hui XW, Gresh N, Pullman B (1990) Modelling of the binding specificity in the interactions of cationic porphyrins with DNA. Nucleic Acids Res 18(5):1109–1114

Jain A, Rajeswari MR (2002) Preferential binding of quinolones to DNA with alternating G, C/A, T sequences: a spectroscopic study. J Biomol Struct Dyn 20(2):291–299

Jasuja R, Jameson DM, Nishijo CK, Larsen RW (1997) Singlet excited state dynamics of tetrakis(4-N-methylpyridyl)porphine associated with DNA nucleotides. J Phys Chem B 101(8):1444–1450. doi:10.1021/jp962684w

Kim JO, Lee YA, Yun BH, Han SW, Kwag ST, Kim SK (2004) Binding of meso-tetrakis(N-methylpyridinium-4-yl)porphyrin to AT oligomers: effect of chain length and the location of the porphyrin stacking. Biophys J 86(2):1012–1017. doi:10.1016/s0006-3495(04)74176-4

Luo Y, Chang CK, Kessel D (1996) Rapid initiation of apoptosis by photodynamic therapy. Photochem Photobiol 63(4):528–534

Magde D, Wong R, Seybold PG (2002) Fluorescence quantum yields and their relation to lifetimes of rhodamine 6G and fluorescein in nine solvents: improved absolute standards for quantum yields. Photochem Photobiol 75(4):327–334

McGhee JD, von Hippel PH (1974) Theoretical aspects of DNA-protein interactions: co-operative and non-co-operative binding of large ligands to a one-dimensional homogeneous lattice. J Mol Biol 86(2):469–489. doi: 10.1016/0022-2836(74)90031-X

Mezo G, Herenyi L, Habdas J, Majer Z, Mysliwa-Kurdziel B, Toth K, Csik G (2011) Syntheses and DNA binding of new cationic porphyrin-tetrapeptide conjugates. Biophys Chem 155(1):36–44. doi:10.1016/j.bpc.2011.02.007

Morris GM, Huey R, Lindstrom W, Sanner MF, Belew RK, Goodsell DS, Olson AJ (2009) AutoDock4 and AutoDockTools4: automated docking with selective receptor flexibility. J Comput Chem 30(16):2785–2791. doi:10.1002/jcc.21256

Pasternack RF (2003) Circular dichroism and the interactions of water soluble porphyrins with DNA. Chirality 15(4):329–332. doi:10.1002/chir.10206

Pedretti A, Villa L, Vistoli G (2004) VEGA—an open platform to develop chemo-bio-informatics applications, using plug-in architecture and script programming. J Comput Aided Mol Des 18(3):167–173. doi:10.1023/B:JCAM.0000035186.90683.f2

Pettersen EF, Goddard TD, Huang CC, Couch GS, Greenblatt DM, Meng EC, Ferrin TE (2004) Chimera a visualization system for exploratory research and analysis. J Comput Chem 25(13):1605–1612. doi:10.1002/jcc.20084

Powell MJD (1977) Restart procedures for the conjugate gradient method. Math Progr 12(1):241–254. doi:10.1007/bf01593790

Sari MA, Battioni JP, Dupre D, Mansuy D, Le Pecq JB (1990) Interaction of cationic porphyrins with DNA: importance of the number and position of the charges and minimum structural requirements for intercalation. Biochemistry 29(17):4205–4215

Shieh YA, Yang SJ, Wei MF, Shieh MJ (2010) Aptamer-based tumor-targeted drug delivery for photodynamic therapy. ACS Nano 4(3):1433–1442. doi:10.1021/nn901374b

Steenkeste K, Tfibel F, Perree-Fauvet M, Briandet R, Fontaine-Aupart MP (2010) Tracking the photosensitizing antibacterial activity of mono(acridyl)bis(arginyl)porphyrin (MABAP) by time-resolved spectroscopy. J Phys Chem A 114(9):3334–3339. doi:10.1021/jp910387a

Stewart JJP (2007) Semiempirical molecular orbital methods. In: Reviews in computational chemistry. Wiley, New York, pp 45–81. doi:10.1002/9780470125786.ch2

Strickland JA, Marzilli LG, Gay KM, Wilson WD (1988) Porphyrin and metalloporphyrin binding to DNA polymers: rate and equilibrium binding studies. Biochemistry 27(24):8870–8878. doi:10.1021/bi00424a027

Tada-Oikawa S, Hirayama J, Hirakawa K, Kawanishi S (2009) DNA damage and apoptosis induced by photosensitization of 5,10,15,20-tetrakis (N-methyl-4-pyridyl)-21H,23H-porphyrin via singlet oxygen generation. Photochem Photobiol 85(6). doi:10.1111/j.1751-1097.2009.00600.x

Tjahjono DH, Mima S, Akutsu T, Yoshioka N, Inoue H (2001) Interaction of metallopyrazoliumylporphyrins with calf thymus DNA. J Inorg Biochem 85(2–3):219–228. doi:10.1016/S0162-0134(01)00186-6